Applied Thermal Engineering 102 (2016) 1422–1432

Contents lists available at ScienceDirect

Applied Thermal Engineering

journal homepage: www.elsevier.com/locate/apthermeng

Research Paper

Optimization of thermal design of ribbed flat-plate fin heat sink

Hamdi E. Ahmed

Department of Mechanical Engineering, University of Anbar, Ramadi 31001, Iraq

HIGHLIGHTS

- Thermal design optimization of plate-fin heat sink by using ribs between channels.
- The dimensions, numbers and orientations of the ribs are optimized.
- Equivalent heat transfer obtained by adding ribs and reducing the air pumping power.
- Saving the substrate material by reducing the fins number and adding ribs.
- Heat sink (5 channel, 15 ribs) shows better performance than smooth heat sink (9 channel).

GRAPHICAL ABSTRACT

(Left) isotherm lines, and (right) streamlines contours for (a) $\psi = 1$, and (b) $\psi = 5$ at re = 1500 and $\xi = 1.0$.

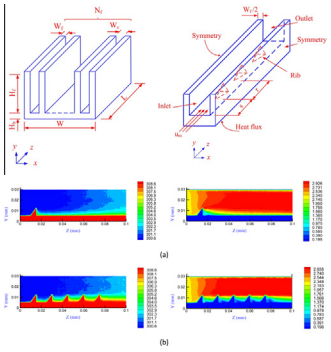

ARTICLE INFO

Article history:
Received 29 December 2015
Revised 6 March 2016
Accepted 19 March 2016
Available online 6 April 2016

Keywords:
Optimization
Thermal design
Plate-fin heat sink
Ribs
Fins

ABSTRACT

Enhancing the thermal design of plate-fin heat sink (PFHS) leads to minimize their size and weight, and then improve the heat removal in consequently increase the speed of electronic devices. In this numerical study, an innovative thermal design of PFHS is suggested by inserting ribs in between channels in different sizes, positions, numbers and orientations in order to get an optimal thermal design of this kind of heat sinks. The two main objectives of this study are; investigating the effect of ribs on PFHS while the number of fins is kept constant, second is inserting ribs with reducing the number of fins simultaneously. Two types of reductions are investigated here, first is substrate material reduction by reducing the number of fins and adding ribs simultaneously, second is pumping power reduction by keeping the number of fins and inserting ribs with reducing the pumping of air flow to get the same thermal performance of the original heat sink (without ribs). The concrete findings show that ribbed plate-fin heat sink (RPFHS) provides thermal performance of 1.55 times greater than PFHS under corresponding conditions. But this enhancement reduces when the number of ribs increases. For the same thermal performance, the pumping power of RPFHS is reduced to 69.65% compared to PFHS case. In addition, RPFHS having five channels with 15 ribs shows hydrothermal performance of 1.37 times better than PFHS having nine channels, with reduction in the substrate material of 27.24%.

1. Introduction

The performance reliability and life expectancy of electronic devices are strongly affected negatively by the component's temperature. The electronic devices are usually cooled by forced air convection because the air cooling is still the most common, simple, reliable, and low cost cooling technique. Investigators are looking for lighter and smaller designs with higher speed of the electronic processers more than old designs. Thus, the rate of heat generated in the high power electronics will increase relatively.

E-mail address: hamdi.ahmed@uoanbar.edu.iq

http://dx.doi.org/10.1016/j.applthermaleng.2016.03.119
1359-4311/

Nomenclature

A	area, m^2
C_p	specific heat, J/kg K
D_h	hydraulic diameter, m
f	friction factor
h	convection heat transfer coefficient, W/m^2 K
H	height, m
JF	performance evaluation criterion
k	thermal conductivity, W/m K
L	length, m
N	number
Nu	Nusselt number
p	pressure, Pa
P.P	pumping power, W
Δp	pressure drop, Pa
PFHS	plate-fin heat sink
q	heat flux, W/m^2
Q	heat transfer, W
$\dot{Q}$	mass flow rate, m^3/s
r	pitch distance of ribs
Re	Reynolds number
RPFHS	ribbed plate-fin heat sink
s	distance between the tip of rib and leading edge of channel, m
T	temperature, K
u, v, w	Velocity components in x, y and z directions, respectively, m/s
VG	vortex generator
W	width, m
x, y, z	Cartesian coordinates in X, Y, and Z direction, respectively
Z	dimensionless axial distance, m

Greek symbols

δ	rib height ratio
θ	dimensionless temperature
μ	dynamic viscosity, kg/m s
ξ	fin reduction ratio
ρ	density, kg/m^3
ψ	rib number ratio

Subscripts

*	modified case
avg	average
b	base of substrate
c	channel
f	fin
f	fluid zone
in	inlet
m	mean
o	original case
R	rib
w	wall

Therefore, more effective and compact cooling systems such as heat sink (HS) is required to avoid reducing the lifespan of electronic components or even causing damage to them. In other words, higher heat removal means possibility of higher performance of electronic systems and consequently improvement of electronic devices speed with keeping their size [1–4].

Li and Shi [1] optimized the thickness of a HS base with different heat transfer boundary conditions. They obtained relationships for forced convection air and liquid working fluids in terms of heat sink area ratios to a heating source, and the lowest thermal resistance. They correlated an equation for these three parameters to optimize the thermal design of the heat sink examined.

Huang and Chen [2,3] and Huang et al. [4] optimized the thermal design of non-uniform fin widths of HS and minimized the thermal resistance of the fin array. Their numerical and experimental results showed that thermal resistance reduction obtained was about 12.7% at Reynolds number (Re = 5000), while Nusselt number (Nu) increased around 14.5% compared to the original heat sink. The thermal performance of optimal impingement heat sinks was significantly improved.

Kim [5], Kim et al. [6] and Li and Chen [7] optimized the thermal performance of a plate-fin heat sink with different widths and heights of fins. They obtained 30% reduction in the thermal resistance compared to the flat plate-fin heat sink. This reduction was increased with increasing of the flow rate and decreasing of the heat sink length. They reported that increasing of the fin width caused a reduction in the thermal resistance initially until a certain value and then increased. Higher fin heights showed lower thermal resistance. As a conclusion, the thermal resistance was significantly reduced by the fin width more than the fin height. Close to the work of Kim and his team, Li et al. [8] remarked that the heat was more uniformly transferred to the base plate by a vapor chamber heat sink than that of a similar aluminum heat sink, and subsequently the maximum temperature was reduced. They also confirmed the reverse relationship between the thermal resistance and Reynolds number. Significant effect of fin dimensions on the thermal performance was observed at lower Reynolds numbers, while at a high Reynolds number, the thermal performance was enhanced as the fin number increased. Chen et al. [9] examined the effect of channel width, fin width, and channel height on the heat sink performance numerically. The results proved that the reduction in both thermal resistance and pressure drop can be obtained by determination of channel configuration and inlet velocity which yields better thermal performance of the heat sink. Mohammadian and Zhang [10] inferred that regardless uniformity of pin fin heights of heat sinks compare to the heat sink without pin fins, not only minimized the bulk temperature inside Lithium-ion battery, but also showed lower standard deviation of the temperature field of the heat sink as well. The standard deviation of the temperature field was decreased when inlet air temperature increased while the maximum temperature of the heat sink was improved. Chen et al. [11] optimized the design of reliable inline and staggered pin–fin heat sink. They found that the increase in the reliability led to make the temperature distribution more symmetric and uniform around the center line of the heat sink and sequentially provided higher ability to resist the environmental variations.

Ahmed and Ahmed [12] examined several geometric parameters of microchannel heat sinks (MCHS) in order to optimize the thermal performance. They proved that the trapezoidal grooved MCHS provided better heat transfer enhancement with low increase in the friction factor compared to the rectangular and triangular grooved heat sinks. Wang et al. [13] examined several types of HS with and without turbulators positioned at the fin surfaces of the heat sinks. Their results indicated that the proposed full cannelure fin along with the dimple/cavity structure provided heat transfer enhancement of 25% with friction reduction of 20%. They stated that the interrupted fins still offer good enhancement in fully developed region without obvious increase in the pressure drop penalty.

Lin et al. [14] examined vertical and oblique planar fin heat sink to create extended surfaces keeping the cross-sectional areas within the fins array. Their experiments revealed that the oblique planar fins heat sink showed better heat transfer rate than that with vertical fins. For high-pressure fan, the extra cooling effect reduced the CPU case temperature about 6 °C using oblique fins. The numerical and experimental results of Shaalan et al. [15] displayed that a shield enhanced the thermal performance of a plate-fin heat sink particularly at low Reynolds number. Moreover, the inclination angle of the shield minimized the thermal resistance and varied with the height of the heat sink. Lowest fin height showed lowest thermal resistance. Whereas Li et al. [16] highlighted that the geometric parameters of vortex generators (VG), which were installed in a cross flow channel before a flat-fin heat sink, such as the distance between the tips of the VG, the distance between each VG and the heat sink, the height, attack angle and configuration of the VG, and the Reynolds number played a vital role in the enhancement of the thermal performance of the HS. They stated that although the heat transfer was enhanced, higher pressure drop was also registered. Yang et al. [17] investigated the performance of heat sinks having fin patterns of delta, semi-circular vortex generators, plain fin and their combinations. They monitored that the heat transfer augmentation by using VG was relatively effective technique when the flow is in the developing region compared to the fully developed region. They stated that the VG operated at a higher frontal velocity and at a larger channel width was more beneficial than that of plate-fin heat sink.

Yu et al. [18] developed the idea of Jonsson and Moshfegh [19] by inserting pins staggered between the plate-fin heat sinks in order to disturb airflows passing through the HS and consequently enhance the thermal performance of the HS. Their numerical and experimental results illustrated that thermal resistance of the HS with pins was 30% lower than that of smooth heat sink. The effectiveness of the heat sinks can be varied by changing the number of pins between the plate-fins. Hasan [20] examined the application of nanofluids in pin–fin (square, triangular and circular pin–fin) microchannel heat sink. A higher heat transfer enhancement was noticed by using nanofluids instead of water particularly by increasing the nanoparticles concentrations associated with an increase in the pressure drop. Shafeie et al. [21] studied the laminar forced convection of micro pin–fin HS cooled by water. It was displayed that for the given pumping power, the heat transfer of the FHS was lower than that in the optimum simple MCHS at medium and high pumping powers. For small pumping powers, the finned heat sink performed slightly better than an optimum simple MCHS.

Li et al. [22] examined vertical Y-shaped bifurcation plates in microchannel heat sink to enlarge the area of heat removal surface. Their results showed better thermal performance for MCHS with this kind of bifurcation compared to the corresponding straight one. The optimal thermal performance obtained was when the angle between the two arms of the Y-shaped plates was kept at 90°. The thermal resistance decreased with the increase of Reynolds number and it was smaller compared to the smooth MCHS associated with a great increase in the pressure drop. Chai et al. [23] examined numerically rectangular ribs inserted in the transverse (interrupted) microchannels heat sink varying the rib length and width and the arrangement of the ribs. They reported that the interrupted microchannel with ribs was good passive method for heat transfer enhancement for $Re < 600$ only.

Wang et al. [24] studied an inverse geometric optimization of nanofluid-cooled microchannel heat sink. They tested the parameters of the number, aspect ratio, and the width ratio of the channels. The thermal performance of microchannel heat sink increased with increasing the pumping power in low power pumping regime. They stated that the use of nanofluid does not always provide better performance for thermal system than base fluids. Xia et al. [25] investigated the micro heat sink having fan-shaped reentrant cavities and internal ribs using water as coolant. They obtained an enhancement in Nusselt number of 1.3–3 times with 6.5 increase in the friction factor compared to smooth rectangular channels. They stated that the effect of rib height was stronger than the individual effect of the size or arrangement of reentrant cavity for $Re > 300$.

Jajja et al. [26] studied the effect of fin spacing on the thermal design of flat plate minichannel heat sink using water as working fluid. Different fin spacing were considered ranged from 0.2 mm to 1.5 mm. They obtained a lowest temperature in the substrate at fin spacing of 0.2 mm. The thermal resistance and heat sink base temperature reduced by decreasing the fin space and increasing *Re* number.

It is clearly observed from above open literature and to the best knowledge of the authors that the optimization of thermal design of the plate-fin heat sink by inserting ribs in the channels seems not to have attention from former investigators. The objective of this paper is to develop the work of Yu et al. [18] and Jonsson and Moshfegh [19] by inserting ribs in the channels in different sizes, numbers, positions and orientations. Two types of reduction are investigated here, first is the substrate material reduction by reducing the number of fins and adding ribs, and second is the pumping power reduction by keeping the number of fins and adding ribs with reducing the pumping of air flow to get the same thermal performance of original heat sink (without ribs). The results of Nusselt number, *JF* factor and streamlines and isotherm lines contours are depicted and illustrated in order to optimize the thermal design of this kind of heat sinks by varying the geometric parameters.

2. Mathematical formulation

2.1. Problem statement and assumptions

The schematic diagram of the physical problem considered in this research is shown in Fig. 1. The area of the bottom of the substrate is $100 \times 100\ mm^2$ (i.e., length (L) × width (W)). The height and the width of the fin are ($H_f = L/4$ and $W_f = 4.6$ mm), respectively. The height of the base of the substrate is ($H_b = 0.05L$). The number of the fins (N_f) of the plain PFHS is 10. The width of the channel is varied along the tests. New design of ribs is suggested and considered in each channel, attached on the bottom of the flow channel. The length and the width of the rib is ($L_R = 0.05L$ and $W_R = 0.04L$), respectively. Three heights are considered for the ribs. The distance between the leading edge of the channel and the tip of the rib (s) is $0.1L$. The range of the varied parameters are shown in Table 1.

The parameters varied along this study are; the height, number and orientation of the ribs, and the number of fins. The first optimization parameter is the rib height ratio which is defined as ($\delta = H_R/H_f$). For the second optimization parameter, the rib number ratio which is mathematically defined as ($\psi = N_R/N_c$). The third optimization parameter is the fin reduction ratio (ξ) which is defined as the new number of fins to the original number of fins (10). Mathematically, ($\xi = N_f^*/N_{f,o}$). Last parameter investigated in this study is the pumping power reduction. The heat flux supplied to the bottom of the substrate block is considered $1500\ kW/m^2$. The geometrical parameters of the PFHS, RPFHS, the computational domain and the rib dimensions are illustrated in Fig. 1(a)–(d), respectively.

Using air as working fluid, the following assumptions are considered for heat transfer and fluid flow characteristics in the RPFHS:

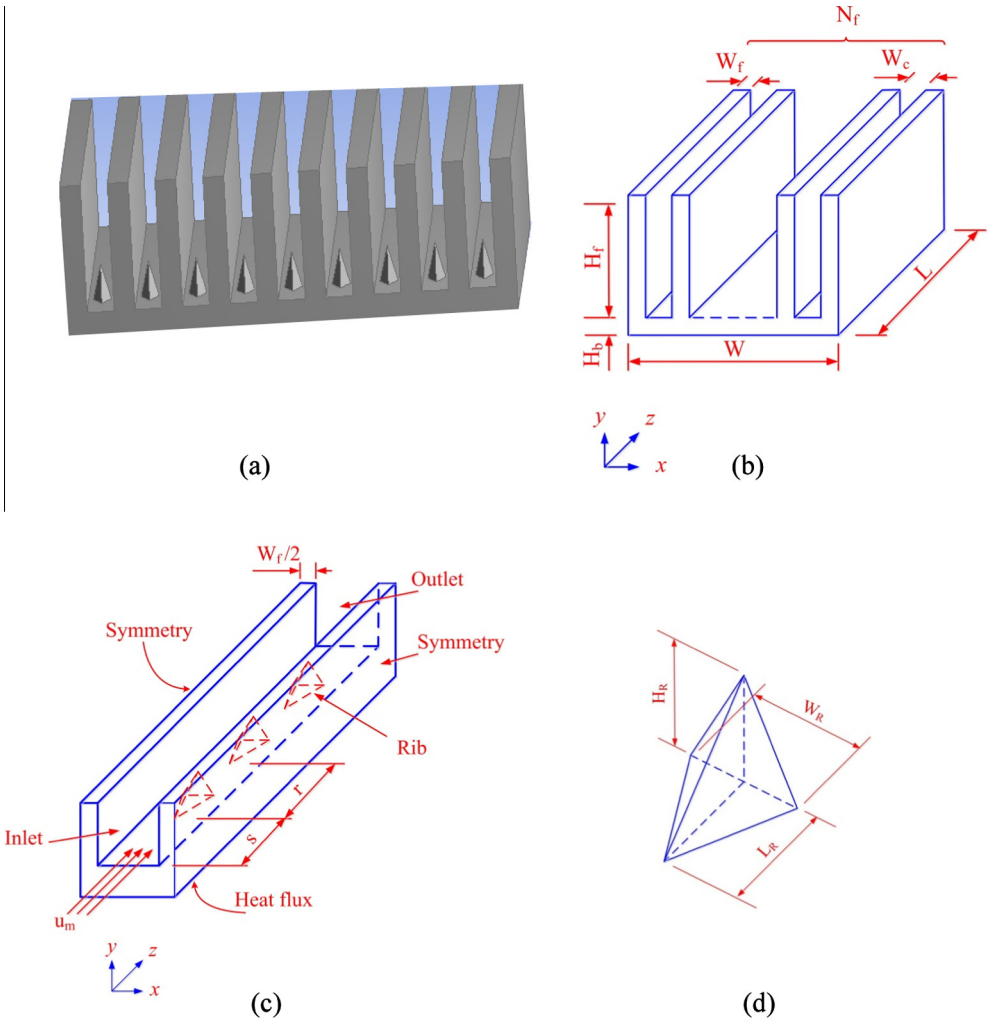

Fig. 1. Schematic diagram of (a) RPFHS, (b) geometric parameters of PFHS, (c) computational domain, and (d) geometric parameters of rib. The scheme is not drawn to scale.

Table 1
Variables of geometric parameters considered for optimization.

Symbol	Equation/note	Domain
W_c	–	6, 9, 14.5 mm
H_R	–	5, 7, 9 mm
N_f	–	10, 8, 6
N_R	In each channel	0, 1, 2, 3, 5
δ	H_R/H_f	0.0, 0.2, 0.28, 0.36
ψ	N_R/N_c	0, 1, 2, 3, 5
ξ	$N_f^*/N_{f,o}$	1.0, 0.8, 0.6
Re	$\frac{\rho u D_h}{\mu}$	200, 500, 850, 1150, 1500

Table 2
Definition of symbols of governing equations, Eq. (1).

Equation	Φ	Ψ	Γ
Continuity	1	0	0
X–momentum	u	$\frac{\mu}{\rho}$	$-\frac{1}{\rho}\frac{\partial p}{\partial x}$
Y–momentum	v	$\frac{\mu}{\rho}$	$-\frac{1}{\rho}\frac{\partial p}{\partial y}$
Z–momentum	w	$\frac{\mu}{\rho}$	$-\frac{1}{\rho}\frac{\partial p}{\partial z}$
Energy (fluid zone)	T_f	$\frac{k}{\rho C_p}$	0
Energy (solid zone) ($u = v = w = 0$)	T_s	$k_{aluminum}$	0

- Three-dimensional fluid flow and steady-state.
- Laminar forced convection heat transfer.
- Negligible radiation heat transfer.

2.2. Governing equations

The continuity, momentum and energy governing equations can be written as

$$\frac{\partial(u\Phi)}{\partial x}+\frac{\partial(v\Phi)}{\partial y}+\frac{\partial(w\Phi)}{\partial z}=\frac{\partial}{\partial x}\left(\Psi\frac{\partial\Phi}{\partial x}\right)+\frac{\partial}{\partial y}\left(\Psi\frac{\partial\Phi}{\partial y}\right)+\frac{\partial}{\partial z}\left(\Psi\frac{\partial\Phi}{\partial z}\right)+\Gamma \quad (1)$$

where Φ stands to the dependent parameters u, v, w and T, and Ψ and Γ are corresponding source and diffusion terms, respectively as tabulated in Table 2. In the above equation, the u, v, and w are the velocity components in x, y and z directions, respectively, and p is pressure and T is temperature.

2.3. Boundary conditions

The boundary conditions for the above set of governing equations are as follows:

Channel inlet	$W_f/2 \leqslant x \leqslant W_c + W_f/2;\ H_b \leqslant y \leqslant H_b + H_f;\ z = 0$	$u = u_{in},\ v = w = 0,\ T = T_{in} = 300$ K
Channel exit	$W_f/2 \leqslant x \leqslant W_c + W_f/2;\ H_b \leqslant y \leqslant H_b + H_f;\ z = L$	$\frac{\partial u}{\partial z} = \frac{\partial v}{\partial z} = \frac{\partial w}{\partial z} = \frac{\partial T_f}{\partial z} = 0,\ p = p_{out} = 1$ atm
Upper wall	$0 \leqslant x \leqslant W_c + W_f;\ y = H_b + H_f;\ 0 \leqslant z \leqslant L$	$u = v = w = 0;\ -k_w \frac{\partial T_w}{\partial Y} = 0$
Internal sidewalls and lower wall of channel	• $x = W_f/2;\ H_b \leqslant y \leqslant H_b + H_f;\ 0 \leqslant z \leqslant L$ • $x = W_c + (W_f/2);\ H_b \leqslant y \leqslant H_b + H_f;\ 0 \leqslant z \leqslant L$ • $W_f/2 \leqslant x \leqslant W_c + (W_f/2);\ y = H_b;\ 0 \leqslant z \leqslant L$	• $u = v = w = 0;\ -k_w \frac{\partial T_w}{\partial X} = q$ • $u = v = w = 0;\ -k_w \frac{\partial T_w}{\partial X} = q$ • $u = v = w = 0;\ -k_w \frac{\partial T_w}{\partial Y} = q$
Lower heated wall of substrate HS	$0 \leqslant x \leqslant W_c + W_f;\ y = 0;\ 0 \leqslant z \leqslant L$	$u = v = w = 0;\ -k_w \frac{\partial T_w}{\partial Y} = q$
Sidewalls of substrate HS (symmetry)	• $x = 0,\ 0 \leqslant y \leqslant H_b + H_f;\ 0 \leqslant z \leqslant L$ • $x = W_c + W_f;\ 0 \leqslant y \leqslant H_b + H_f;\ 0 \leqslant z \leqslant L$	$\frac{\partial u}{\partial x} = \frac{\partial w}{\partial x} = \frac{\partial T_f}{\partial x} = \frac{\partial T_w}{\partial x} = 0,\ v = 0$
Front and back wall of substrate HS	• $0 \leqslant x \leqslant W_c + W_f;\ 0 \leqslant y \leqslant H_b + H_f;\ z = 0$ • $0 \leqslant x \leqslant W_c + W_f;\ 0 \leqslant y \leqslant H_b + H_f;\ z = L$	$-k_w \frac{\partial T_w}{\partial Z} = 0$

2.4. Grid independent test

A grid independence test is performed for the simulation domain to find optimum mesh concentration that has high enough mesh elements, give accurate outcomes and save the simulation time. Five different sizes of grid are tested to check the effect of the grid density on the computational results. The nodes of the domain are shown in Table 3. The results show that the grid size of 76,000 provides the same result and smaller computational time. It is worthy to be mentioned that the percentage error for Nusselt number and friction factor is tabulated in Table 1 and calculated using the following formula

$$E_M\% = \left|\frac{M_{max} - M_{min}}{M_{max}}\right| \times 100 \tag{2}$$

where the subscript M represents any parameter.

3. Numerical procedure

3.1. Solution method

The finite volume method (FVM) is used to solve the governing equations with corresponding boundary conditions by using the commercial computational fluid dynamics (CFD) package (FLUENT v12.1). The convective term of 2nd order upwind method implementing the SIMPLE algorithm is employed for the pressure and velocity coupling. The diffusion term in the momentum and energy equations is approximated by 2nd order upwind. A non-uniform structured mesh is generated for the whole domain except the zone of ribs in which non-uniform, unstructured, finer and high concentration mesh is applied. The iteration of simulations was continued until the sum of normalized residual of all components became negligible (less than 10^{-5}) and velocity components did not alter from each other iteration. The residual sum for each of the conserved variables is computed and stored at the end of each iteration, thus recording the convergence history. Moreover, the convergence criterion demanded that the maximum relative mass residual based on the inlet mass be smaller than 10^{-10}.

Table 3
Grid independence test.

Grid number	Nu_{avg}	$E_{Nu}\%$	f	$E_f\%$
36,000	3.1400	–	0.4295	–
47,600	3.1067	1.072	0.4397	2.3187
76,000	3.1094	0.087	0.4468	1.6037
110,680	3.1070	0.077	0.4559	1.9988
264,000	3.1095	0.081	0.4634	1.6001

3.2. Numerical calculation

The convection heat transfer coefficient and local Nusselt number are estimated as follows, respectively

$$h = \frac{Q}{A_h(\overline{T}_w - \overline{T}_a)} \tag{3}$$

$$Nu_z = \frac{h_z D_h}{k} \tag{4}$$

where $A_h, \overline{T}_w$ and $\overline{T}_a$ are the convection heat transfer area, the average heated wall temperature and the average air bulk temperature, respectively. The A_h is estimated by

$$A_h = (2H_f + W_c) \times L \tag{5}$$

Reynolds number is calculated from the following formula

$$Re = \frac{\rho \cdot u \cdot D_h}{\mu} \tag{6}$$

where D_h is the hydraulic diameter of the channel which is calculated as follows

$$D_h = 4\frac{A_c}{P} = 2\frac{W_c \cdot H_f}{(W_c + H_f)} \tag{7}$$

where A_c represents the cross-sectional area of the channel flow and P represents the wetted perimeter of the channel. The friction factor in the duct is calculated by

$$f = \frac{2D_h \Delta p}{L_c \rho u_m^2} \tag{8}$$

The hydrothermal performance evaluation factor (JF) is defined as the ratio of modified Nusselt number of RPFHS to that of PPFHS to the modified friction factor to that of PPFHS. In mathematical formula [27]

$$JF = \frac{(Nu^*/Nu_o)}{(f^*/f_o)^{\left(\frac{1}{3}\right)}} \tag{9}$$

The pumping power (P.P) required to propel a volumetric flow rate ($\dot{Q}$) through the pressure drop Δp is estimated from

$$P.P = \dot{Q} \times \Delta p = u_m \times A_c \times \Delta p \tag{10}$$

where the cross-sectional area for one channel is calculated by

$$A_c = H_f \times W_c \tag{11}$$

4. Results and discussion

As explained earlier, the main objective of the current study is to optimize the thermal design of flat-plate fin heat sink by using new design of ribs. This optimization is planned to be achieved by considering three main goals; first is enhancing the thermal design of the heat sink, second is saving the substrate material by reducing the number of fins and replacing them by ribs, and the third goal is investigating the pumping power reduction when the ribs are used in between the fins. For the first goal, several parameters are considered; the height, the number and position of ribs. While for the second goal, the reducing the fins' numbers and adding ribs were the variables. Before doing the present simulations, set of CFD simulation validation was performed in order to make sure the accuracy of the current results as in the following section.

4.1. Validation of plate-fin heat sink

The present CFD model is first validated with the recent experimental results of Sohel et al. [28] for mini-channel plate-fin heat sink. The comparison is performed with the average convection heat transfer coefficient (h) and pumping power (P.P) are shown in Fig. 2(a) and (b), respectively. The deviations between the present numerical results and the experimental data of Sohel are 5.07% and 10.78%, respectively with the above parameters. In addition, the present numerical model is validated with the correlations of Phillips [29] and Steinke and Kandlikar [30] under same boundary conditions as shown in Fig. 2(c) and (d), respectively. The deviation in the last two subfigures are 9.61% and 5.91%, respectively. More details about these correlations are reported by Ahmed and Ahmed [12].

It is worth to be mentioned that the symbol Z of the abscissa of Fig. 2(c) is defined as

$$Z = \frac{z}{D_h Re_{D_h} Pr} \tag{12}$$

where Pr is Prandtl number.

The comparative figures show that the present numerical data is close to the results of the open literature with an acceptable deviation. The deviation can be attributed to the uncertainties of the previous experimental result. Generally, it can be clearly seen the good agreement between the present results and relevant literature.

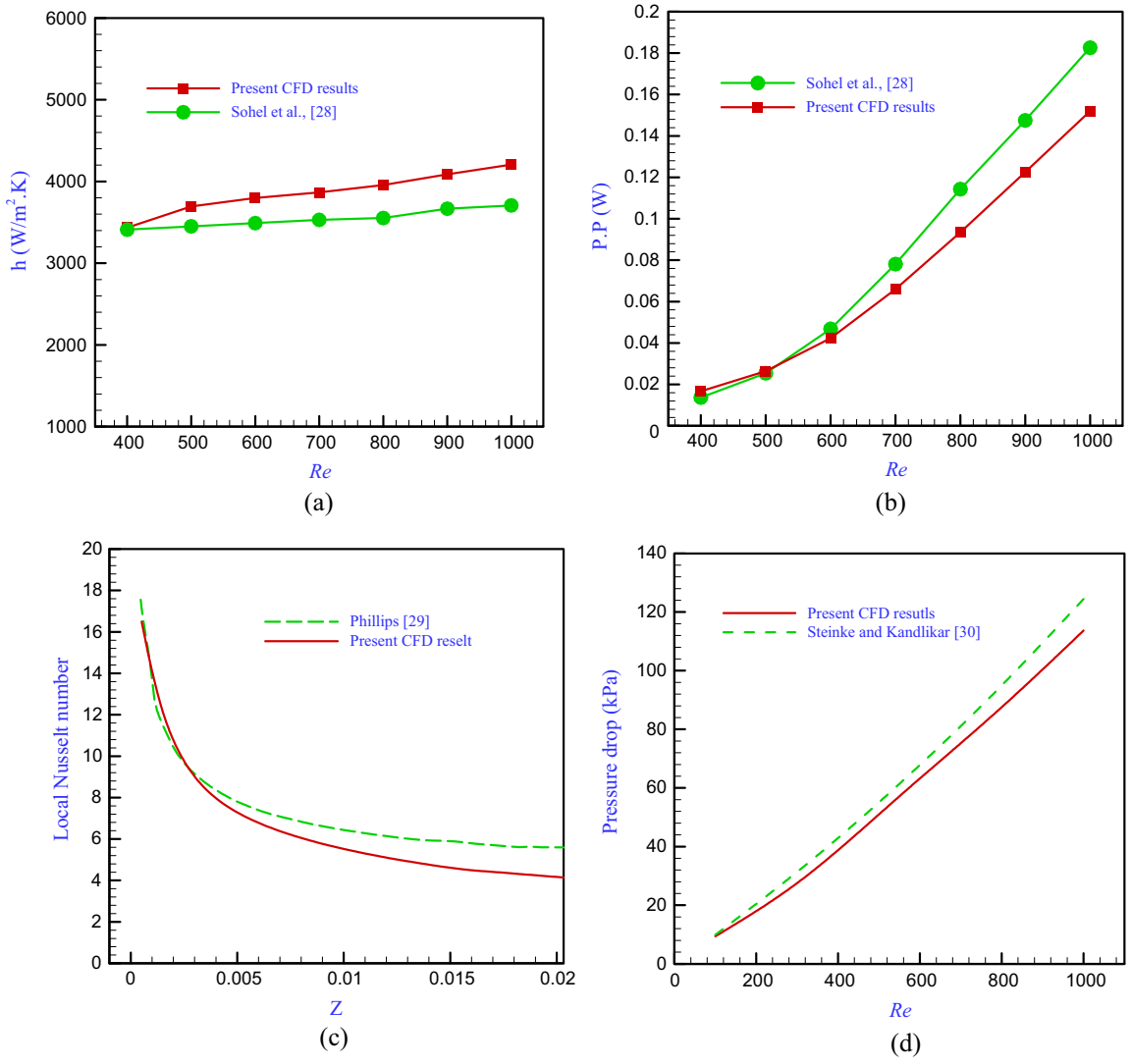

Fig. 2. Validation of present numerical model with the literatures.

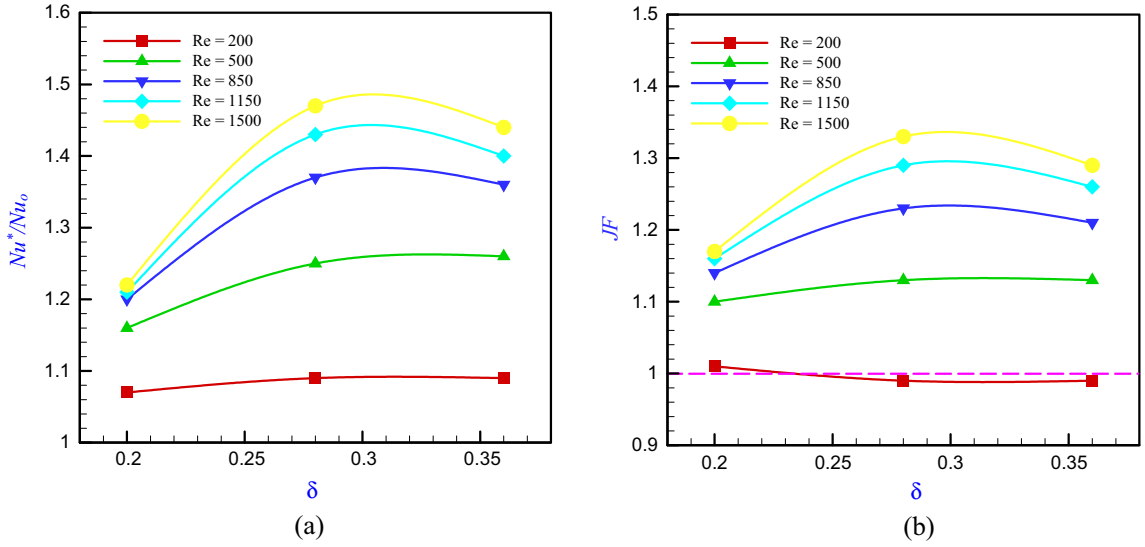

Fig. 3. Effect of rib height ratio δ on (a) average Nusselt number, and (b) *JF* factor at $\psi = 0.1$ and $\xi = 1.0$.

4.2. Effect of rib height ratio (δ)

The height of rib plays an important role in heat transfer enhancement by disturbing the growth of thermal boundary layer. At low Reynolds number, some portion of the height of the rib is embedded in the boundary layer without any effect on the thermal performance but only on the hydraulic performance due to the additional pressure drop. The effect of the height parameter (δ) on the Nusselt number ratio (Nu^*/Nu_o) and *JF* factor is shown in Fig. 3(a) and (b) at $\psi = 0.1$ and $\xi = 1.0$ and for wide range of Reynolds numbers. From this figure, it is clearly seen that the Nusselt number ratio increases explicitly when the rib height ratio increases from 0.20 to 0.28 and then reduces after that. This performance becomes more obvious at highest values of Reynolds numbers. It can be attributed to the fact that when δ increases from 0.20 to 0.28, air separation occurs behind the rib causing swirl in the channel flow and mixing between the cold air at the center of the channel and the hot air layers adjacent to the heated channel surfaces. In that case, the circulation of the flow leads to better mixing between the cold and hot air layers and reduce the thermal boundary layer at the heated walls of the channel. But in contrast, this circulation of fluid becomes meaningless at $\delta = 0.36$ causing only deterioration in the flow with additional pressure drop. In addition, the separation of fluid layers behind the rib, particularly at higher values of Reynolds number, makes the heated surface area like a dead region due to the thick boundary layer behind the rib. This can be clearly seen in the form of isotherm lines and streamlines contours as illustrated in Fig. 4(a) and (b).

By going back to Fig. 3(b), the hydrothermal performance represented by *JF* factor is lower than unit only for $Re = 200$. It can be

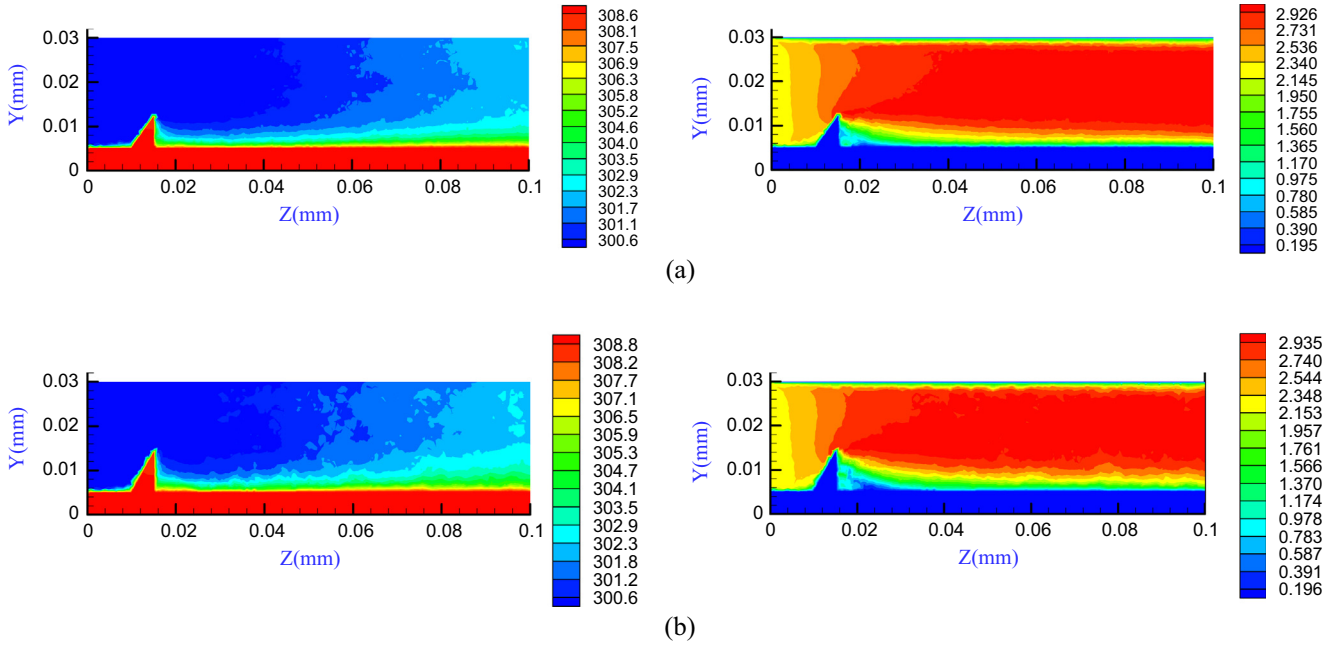

Fig. 4. (Left) Isotherm lines, and (right) streamlines contours for (a) $\delta = 0.28$ and (b) $\delta = 0.36$ at $Re = 1500$, at $\psi = 0.1$ and $\xi = 1.0$.

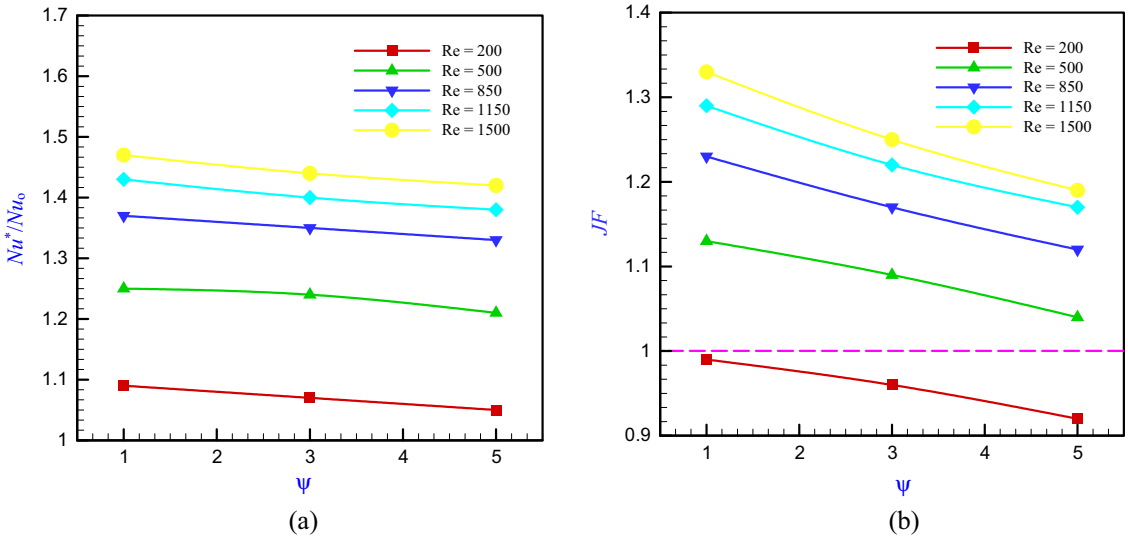

Fig. 5. Effect of rib number ψ on (a) Nusselt number ratio, and (b) *JF* factor at $\delta = 0.2$ and $\xi = 1.0$.

said here that there is a small enhancement in the Nusselt number for all range of δ, while there is an additional drop in the flow loses. This is due to the fact that a part of the height of the rib is still immersed in the boundary layer and it has not any effect to reduce the thermal resistance. In that case, this kind of ribs is not useful at low flow rates.

4.3. Effect of rib's number (ψ)

The second parameter investigated here is the rib number ratio ψ. Fig. 5 shows the effect of ψ on the Nusselt number ratio and *JF* factor for wide range of Reynolds numbers at $\delta = 0.28$ and $\xi = 1.0$. Generally, Nusselt number ratio decreases with increasing ψ with further pumping power causing higher pressure drop. For all cases and for the whole range of Reynolds number, the optimum case is the single rib ($\psi = 0.1$) in each channel while adding further number for ribs means only deterioration for the flow without enhancement in heat transfer. In fact, indeed the inserting of ribs in the channel causes a turbulence in the main flow direction leads to greater heat removal. Besides, adding ribs means further heat transfer surface area. But, each rib creates a stagnation zone behind it. The separation flow in the stagnation zones makes a thick thermal boundary layer and then rise the thermal resistance. Fig. 5(b) confirmed that the optimal thermal design of RPFHS cannot be obtained at low Reynolds number under the current conditions.

The isotherm and stream lines contours for single and five ribs are depicted in Fig. 6(a) and (b). The figure shows that there is no thermal effect when more than single rig ($\psi > 1$) is used, while only additional pumping power required for forcing the fluid in the heat sink. In other words, the ribs after the first row deteriorate the turbulence in the flow in which eddies of air are disrupted, preventing formation of vortices. This results gives an indication that there is not benefit comes from adding more than one rib only extra mechanical operations, additional material, extra costs, and further pumping power. It would be suggested to examine the pitch of ribs in longer heat sinks.

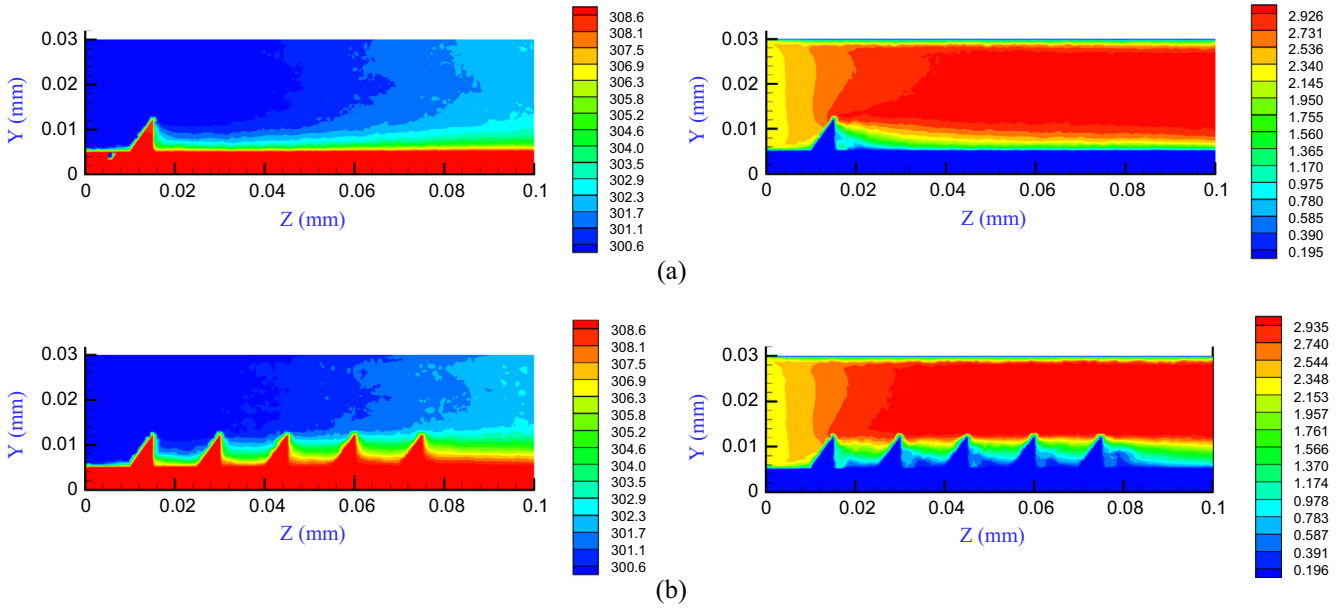

Fig. 6. Top view of (Left) isotherm lines, and (right) streamlines contours for (a) $\psi = 1$, and (b) $\psi = 5$ at Re = 1500 and $\xi = 1.0$.

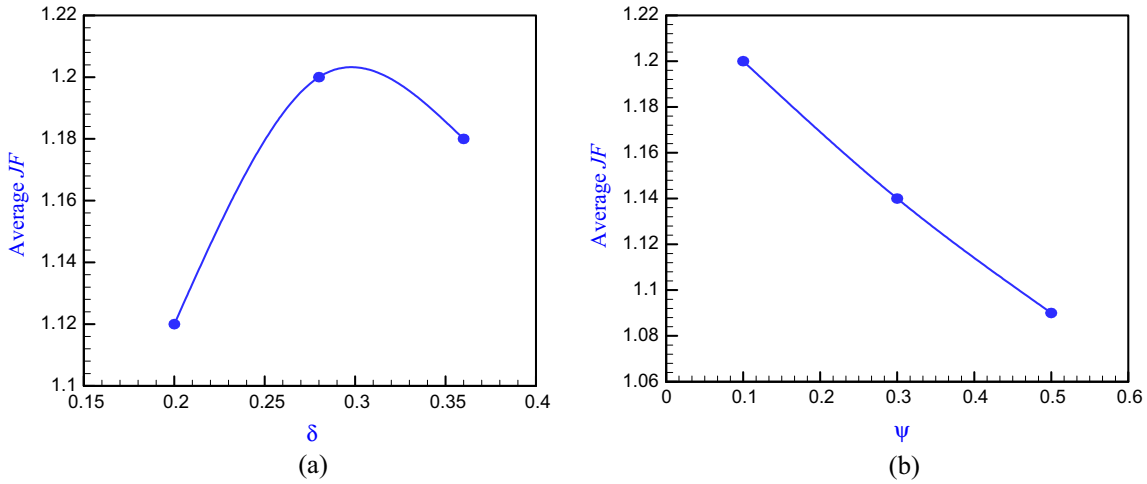

Fig. 7. (a) Effect of rib number δ, and (b) rib height ψ, on the average JF factor at $\xi = 1.0$.

To show the overall performance of the two parameters, δ and ψ, the average JF factor is estimated and depicted as illustrated in Fig. 7(a) and (b). It can be said here that the optimum rib height ratio is $\delta = 0.28$, and the optimal rib number ratio is $\psi = 0.1$. In other words, there is not hydro/thermal enhancement from increasing the rib height ratio greater than 0.28 or using ribs more than one rib for each channel in the case of $\xi = 1.0$.

4.4. Power reduction

In the last part of the current study is to examine the effect of using single rib in each channel with $\delta = 0.28$, $\psi = 1$ and $\xi = 1.0$, on the pumping power reduction. For the case of smooth channel, Nusselt number is 8.7 at Re = 1500. By using rib, the Nusselt number ratio is greatly enhanced as shown in the previous figures. To get the same value of Nusselt number of smooth channel (i.e., $Nu^*/Nu_o = 1$), the flow rate must be reduced when the rib is used. By this way, Reynolds number is reduced up to 795 for the ribbed channel to provide same thermal performance of smooth one. It could be deduced that the pumping power required for pushing the fluid in PPFHS decreases in the case of RPFHS for the corresponding amount of the heat transfer rate. In that case, a reduction in the pumping power is obtained around 69.65% as shown in Table 4.

4.5. Fin number reduction (ξ)

In this section, the optimization of thermal design is achieved by reducing the number of fins and simultaneously adding ribs. The number of ribs in each channel depends on the ratio of ξ as illustrated in Fig. 8(a)–(c). The value of s is kept constant throughout the study, while the distance between the adjacent ribs (t), pitch distance between two rows of ribs (r) and W_c are varied taking in the account the design of the channel and orientation of ribs as shown in Table 5.

Table 4
Pumping power reduction by using rib.

variables	No rib	Ribbed
Nu	8.7	8.7
Re	1500	795
u (m/s)	2.26	1.20
ΔP (Pa)	3.499	2.016
Pumping power (W)	0.010675	0.00324
Power reduction (%)	–	69.65

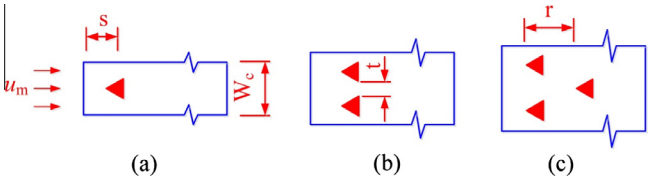

Fig. 8. Top view of position and orientation of ribs for (a) $\xi = 1.0$ and $\psi = 1$, (b) $\xi = 0.8$ and $\psi = 2$, and (c) $\xi = 0.6$ and $\psi = 3$. The scheme is not drawn to scale, and the flow direction is from left to right.

Table 5
Geometric parameters of fin number ratio ξ. All dimensions in (mm).

ξ	ψ	W_c	t	r	s
1.0	1	6.0	–	–	10
0.8	2	9.0	0.5	–	10
0.6	3	14.5	2.5	20	10

Table 6
Geometric parameters of ξ with number of fins and ribs.

Variables	Estimation	$\xi = N_{newfins}/10$		
		1.0	0.8	0.6
N_f	–	10	8	6
N_R	–	Non	2	3
	–	1		
V_f (mm^3)	$W_f \times H_f \times L$	0.00	−23,000	−46,000
V_R (mm^3)	$0.5 \times W_r \times H_r \times L_r \times N_{rib}$	+630	+980	+1050
V_{Total} (mm^3)	$V_f - V_R$	−630	+22,020	+44,950
V_{Sub} (%)	$R_{sub} = \lvert \frac{V_{original} - V_{new}}{V_{original}} \rvert \times 100$	−0.38	+13.34	+27.24

It is worthy to be explained here that the method used in the fin reduction and ribs addition is shown in Table 6. Three values of fin number reduction ratio are examined in this study, namely $\xi = 1.0$, 0.8, and 0.6. Because the channel width increases with increasing the value of ξ, more than one rib is added in the channel in various positions and orientations. It is necessary to calculate the volume of the fins which is reduced from the overall volume of the heat sink, and the total volume of ribs added to the heat sink at the same time. It can be said that the fins removed from the heat sink are assumed profit and material saving, while the ribs added to the

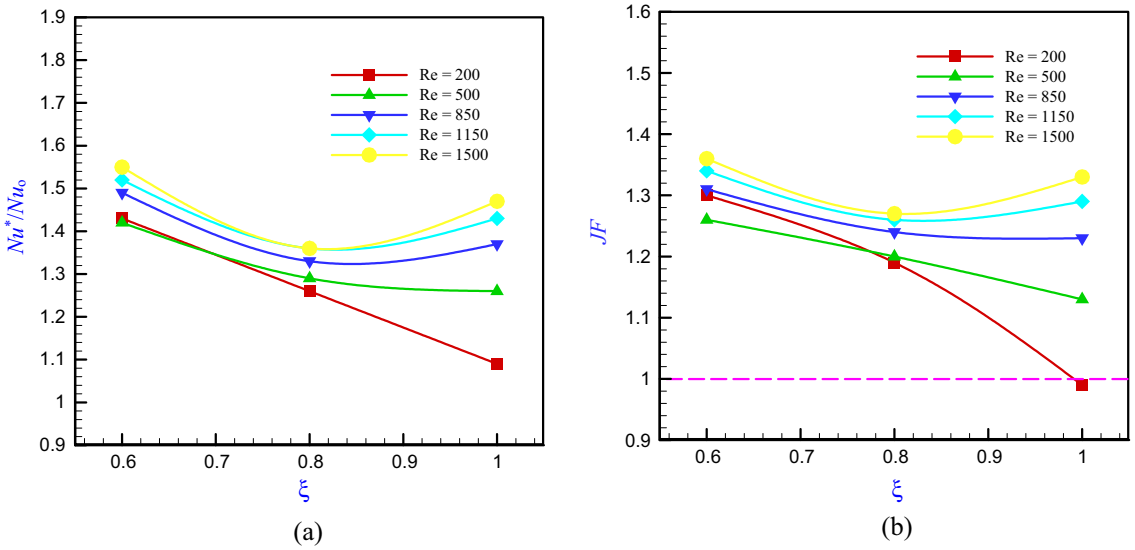

Fig. 9. Fin number reduction ξ, (a) Nusselt number ratio, and (b) JF factor for $\delta = 0.28$.

heat sink is considered as losses material. For this reason, the volume of fin reduction is represented by minus signal whereas the rib volume is represented by plus signal. Finally, the total substrate material reduced by this optimization design is shown in Table 6. Mathematically, the volume of fins removed from the original volume of the substrate material is estimated as

$$V_{\text{f, removed}} = (10 - N_f) \times V_f \tag{13}$$

where V_f is illustrated in Table 6. The number of channel is calculated from

$$N_c = N_f - 1 \tag{14}$$

$$\text{Material reduction } (\%) = R_{sub} = \left| \frac{V_{\text{original}} - V_{\text{new}}}{V_{\text{original}}} \right| \times 100 \tag{15}$$

Where V_f and V_R represent the reduction in the fin material and rib material, respectively.

It should be noted that the case of $\xi = 1.0$ is with and without rib. While for $\xi = 0.8$, two ribs are attached on the bottom of the channel in transvers orientation with the flow direction, and in the case of $\xi = 0.6$, three ribs are installed in each channel with triangular orientation where the base of triangular is facing to the flow direction as shown in Fig. 8(b). Now, a set of simulations is cured out at $\delta = 0.28$ for different values of Reynolds numbers as shown in Fig. 9(a) and (b).

The first group of simulations is to use a single rib in each channel attached in the centerline of the channel bottom ($\xi = 1.0$ and $\psi = 1$). It is emphasized that there is an increase in the pressure drop penalty greater than the enhancement in the Nusselt number at $Re = 200$. That means the use of single rib is not useful because of the thick thermal boundary layer (i.e., high thermal resistance). In contrast, a remarkable thermal enhancement is noticed with increasing of Re number compared to the increase in the frictional losses. For the cases of $\xi = 0.8$ and $\psi = 2$, in general and for the whole range of Reynolds numbers, the hydrothermal performance of the heat sink is quite enormous. For the comparison and for the case of $\xi = 1.0$, the enhancement in hydrothermal performance is better than that of $\xi = 0.8$ at the highest values of Reynolds number only, but in contrast, there is volume reduction in the substrate material about 13.34% in the case of $\xi = 0.8$. It can be attributed to the fact that even there is a reduction in the fins number (two fins removed) but 14 ribs are added (two ribs in each channel) instead of 9 which disturb the growth of the thermal boundary layer and consequently reduce the thermal resistance. For the case of ($\xi = 0.6$), the best hydrothermal performance of the heat sink observed is for the case of 6 fins and 15 ribs (3 ribs in each channel) particularly for high Reynolds numbers. This good performance gives an indication that RPFHS with five channels provides thermal performance about 1.4–1.55 times with nine channels, and hydrothermal performance about 1.26–1.37 times better than original heat sink (without ribs) with reduction in the substrate material around 27.24%. Finally, better hydrothermal performance can be obtained by using RPFHS with $\xi = 0.6$ and $\psi = 3$ instead of smooth channel heat sink having ten fins under same conditions.

It is worth to be mentioned here that the results of Shaalan and his group [15] showed that the thermal performance of HS increased with increasing the fin numbers under turbulent flow regime. But besides, additional pressure drops were registered with the thermal enhancement. In this study, it is proved that the thermal performance of the HS can be improved by reducing the fin numbers and adding ribs in the channels. In contrast, the present results agree well with the results of Li et al. [16] in terms of hydrothermal performance of PFHS, which was increased with using turbulators. In addition, the present results show that the enhancement of hydrothermal performance in large values of ξ is greater than that of small ones, and they agree with the results of Yang et al. [17] due to the short width of the channel which prevents the formation of vortices. Furthermore, the results obtained by Ahmed and Ahmed [12] illustrated that increasing the number of grooves does not mean enhancing the thermal performance, but additional machining processes and further costs. Their results support the present findings.

5. Conclusion

The main aim of this numerical work is to optimize the hydrothermal performance of ribbed plate-fin heat sink RPFHS by considering an innovative design of ribs installed in the channels. Different sizes, numbers, positions and orientations of ribs are investigated. The reduction in the fin number and adding ribs is also explored. The effect of these parameters on the reduction of substrate material is examined. The CFD results can be concluded briefly as follows

- The best hydrothermal performance is observed at the rib height ratio of $\delta = 0.28$, while the performance is reduced at higher and lower than this value.

- The RPFHS provides better hydrothermal performance than smooth one. This performance is monitored higher at rib number ratio of $\psi = 1$, and decreases when this ratio increases.
- It is observed that the fin number ratio of $\xi = 0.6$ and $\psi = 3$ shows best Nusselt number ratio (1.55 times) and *JF* factor (1.37 times) compared to smooth channel heat sink with reduction in the substrate material about 27.24%.
- Maximum pumping power reduction obtained is about 69.65% for the ribbed channel with $\delta = 0.28$, $\psi = 1$ and $\xi = 1.0$ compared to the corresponding original channel heat sink.

Finally, it is strictly encouraged that this area of research still needs a lot of investigations in order to get better thermal design and performance for the flat-plat fin heat sinks particularly for the case of fin reduction and varying the orientation of the ribs.

References

[1] J. Li, Z. Shi, 3D numerical optimization of a heat sink base for electronics cooling, Int. Commun. Heat Mass Transfer 39 (2012) 204–208.
[2] C. Huang, Y. Chen, An impingement heat sink module design problem in determining simultaneously the optimal non-uniform fin widths and heights, Int. J. Heat Mass Transf. 73 (2014) 627–633.
[3] C. Huang, Y. Chen, An optimal design problem in determining non-uniform fin heights and widths for an impingement heat sink module, Appl. Therm. Eng. 63 (2014) 481–494.
[4] C. Huang, Y. Chen, H. Li, An impingement heat sink module design problem in determining optimal non-uniform fin widths, Int. J. Heat Mass Transf. 67 (2013) 992–1006.
[5] D. Kim, Thermal optimization of branched-fin heat sinks subject to a parallel flow, Int. J. Heat Mass Transf. 77 (2014) 278–287.
[6] D. Kim, J. Jung, S.J. Kim, Thermal optimization of plate-fin heat sinks with variable fin thickness, Int. J. Heat Mass Transf. 53 (2010) 5988–5995.
[7] H. Li, K. Chen, Thermal performance of plate-fin heat sinks under confined impinging jet conditions, Int. J. Heat Mass Transf. 50 (2007) 1963–1970.
[8] H. Li, M. Chiang, C. Lee, W. Yang, Thermal performance of plate-fin vapor chamber heat sinks, Int. Commun. Heat Mass Transfer 73 (2010) 731–738.
[9] Y. Chen, B. Peng, X. Hao, G. Xie, Fast approach of Pareto-optimal solution recommendation to multi-objective optimal design of serpentine-channel heat sink, Appl. Therm. Eng. 70 (2014) 263–273.
[10] Sh.K. Mohammadian, Y. Zhang, Thermal management optimization of an air-cooled Li-ion battery module using pin-fin heat sinks for hybrid electric vehicles, J. Power Sources 273 (2015) 431–439.
[11] C. Chen, M. Chen, W. Horng, Reliability-based design optimization of pin-fin heat sinks using a cell evolution method, Int. J. Heat Mass Transf. 79 (2014) 450–467.
[12] H.E. Ahmed, M.I. Ahmed, Optimum thermal design of triangular, trapezoidal and rectangular grooved microchannel heat sinks, Int. Commun. Heat Mass Transfer 66 (2015) 47–57.
[13] C. Wang, K. Yang, Y. Liu, I.Y. Chen, Effect of cannelure fin configuration on compact aircooling heat sink, Appl. Therm. Eng. 31 (2011) 1640–1647.
[14] S. Lin, F. Chuang, Ch. Chou, Experimental study of the heat sink assembly with oblique straight fins, Exp. Thermal Fluid Sci. 29 (2005) 591–600.
[15] M.R. Shaalan, M.A. Saleh, O. Mesalhy, M.L. Elsayed, Thermo/fluid performance of a shielded heat sink, Int. J. Therm. Sci. 60 (2012) 171–181.
[16] H. Li, C. Chen, Sh. Chao, G. Liang, Enhancing heat transfer in a plate-fin heat sink using delta winglet vortex generators, Int. J. Heat Mass Transf. 67 (2013) 666–677.
[17] K. Yang, J. Jhong, Y. Lin, K. Chien, Ch. Wang, On the heat transfer characteristics of heat sinks: with and without vortex generators, IEEE Trans. Compon. Packag. Technol. 33 (2010) 391–397.
[18] X. Yu, J. Feng, Q. Feng, Q. Wang, Development of a plate-pin fin heat sink and its performance comparisons with a plate fin heat sink, Appl. Therm. Eng. 25 (2005) 173–182.
[19] H. Jonsson, B. Moshfegh, Modeling of the thermal and hydraulic performance of plate fin, strip fin, and pin fin heat sinks—influence of flow bypass, IEEE Trans. Compon. Packag. Technol. 24 (2001) 142–149.
[20] M.I. Hasan, Investigation of flow and heat transfer characteristics in micro pin fin heat sink with nanofluid, Appl. Therm. Eng. 63 (2014) 598–607.
[21] H. Shafeie, O. Abouali, K. Jafarpur, G. Ahmadi, Numerical study of heat transfer performance of single-phase heat sinks with micro pin-fin structures, Appl. Therm. Eng. 58 (2013) 68–76.
[22] Y. Li, F. Zhang, B. Sunden, G. Xie, Laminar thermal performance of microchannel heat sinks with constructal vertical Y-shaped bifurcation plates, Appl. Therm. Eng. 73 (2014) 185–195.
[23] L. Chai, G. Xia, M. Zhou, J. Li, J. Qi, Optimum thermal design of interrupted microchannel heat sink with rectangular ribs in the transverse microchambers, Appl. Therm. Eng. 51 (2013) 880–889.
[24] X. Wang, B. An, L. Lin, D. Lee, Inverse geometric optimization for geometry of nanofluid-cooled microchannel heat sink, Appl. Therm. Eng. 55 (2013) 87–94; R.L. Webb, N.H. Kim, Principles of Enhanced Heat Transfer, 2nd edition., Taylor & Francis Group, New York, NY, 2006.
[25] G. Xia, Y. Zhai, Z. Cui, Numerical investigation of thermal enhancement in a micro heat sink with fan-shaped reentrant cavities and internal ribs, Appl. Therm. Eng. 58 (2013) 52–60.
[26] S.A. Jajja, W. Ali, H.M. Ali, A.M. Ali, Water cooled minichannel heat sinks for microprocessor cooling: Effect of fin spacing, Appl. Therm. Eng. 64 (2014) 76–82.
[27] R.L. Webb, N.H. Kim, Principles of Enhanced Heat Transfer, 2nd edition., Taylor & Francis Group, New York, NY, 2006.
[28] M.R. Sohel, S.S. Khaleduzzaman, R. Saidur, A. Hepbasli, M.F.M. Sabri, I.M. Mahbubul, An experimental investigation of heat transfer enhancement of a minichannel heat sink using Al_2O_3–H_2O nanofluid, Int. J. Heat Mass Transf. 74 (2014) 164–172.
[29] R.J. Phillips, Microchannle Heat Sinks, in: Advances in Thermal Modeling of Electronic Components and Systems, Hemisphere Publishing Corporation, New York, NY, 1990 (Chapter 3).
[30] M.E. Steinke, S.G. Kandlikar, Single-phase liquid friction factors in microchannels, Int. J. Therm. Sci. 45 (2006) 1073–1083.